Chapter 12

Injection

12.1 Linac

12.1.1 Overview

To allow for the smooth operation of KEKB, a major upgrade program is under way for the 2.5 GeV injector linac, which was formerly used to inject beams to the Tristan accelerator complex and the Photon Factory (PF) ring. Two main goals of the upgrade are:

- Increase the energies of electrons and positrons to 8 GeV and 3.5 GeV, so that they can be injected into HER and LER of KEKB at full energies.
- Increase the bunch intensities of positrons by a factor of ~ 20 for efficient fills.

Tables 12.1(1) through (4) compare the parameters of the injector before and after the upgrade. The upgrade program includes tasks in the following three areas:

1. Successive replacement of the RF power sources by higher-power klystrons with RF pulse compressors.
2. Small extension of the linac total length.
3. Relocation of the positron production target, so that positrons are produced by incident electrons of 3.7 GeV instead of the former 0.25 GeV.

The pre-upgrade linac consists of six sectors called P, 1, 2, 3, 4 and 5. A regular sector consists of eight accelerator units, which include four 2-m accelerator sections. The accelerator sections in each unit are driven by one klystron. In the upgrade, two sectors will be added to the linac, and they will be renamed A, B, C, 1, 2, 3, 4 and 5, as shown in Figure 12.1.

Sectors A, B and C are those to be newly built. Sector A will have a pre-injector, which will produce intense single bunches. It will include double sub-harmonic bunchers (SHB's), followed by three accelerator units. Sectors B and C are regular accelerating sectors. Sector 2 will be rebuilt so as to include a positron generator by moving Sector P to this location. In Sectors 1, 3, 4 and 5, the component layout will not be changed, or changed only slightly.

The pulse energy of the pulse modulators will be increased by a factor of two. This will be achieved by increasing the total capacitance of PFN while maintaining the same charging voltage. All of the 30-MW klystrons will be replaced by 50-MW types. RF pulse-compressors will be installed at the klystron output with a small modification to the waveguide system and improvements to the vacuum system.

The number of accelerator units is to be increased from 46 to 57. The average energy gain of one unit will be 160 MeV. The full linac energy without beam loading will reach about 9 GeV. An extra energy gain of over 8 GeV(13%) will be used to compensate for any gain loss due to defective units, energy-spread adjustment, or energy tuning.

In the pre-upgrade linac the positrons were produced with primary electrons of 0.25 GeV. The positron production yield has been measured to be $N^+/(N^-E^-) = 1.8$ % GeV^{-1}. The expected positron charge after the upgrade is 0.67 nC for a primary electron pulse of 0 nC at 3.7 GeV.

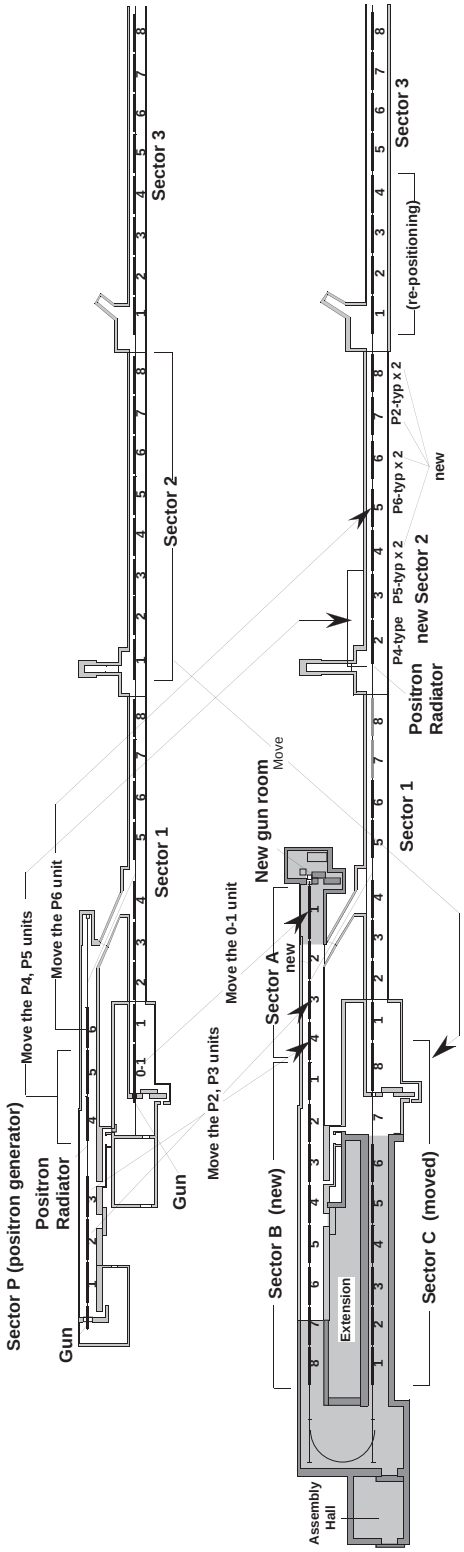

Figure 12.1: Linac re-formation from the 2.5 GeV linac (upper) to the KEKB 8 GeV injector (lower).

		PRESENT	KEKB	
[INJECTION BEAM]				
energy	(e^-)	2.5	8.0	GeV
	(e^+)	2.5	3.5	GeV
pulse length		<2	single bunch	ns
bunch width (σ_z)		∼5	∼5	ps
particle (charge)/pulse	(e^-)	2×10^9(0.32)	8×10^9(1.28)	(nC)
	(e^+)	2×10^8(0.032)	4×10^9(0.64)	(nC)
pulse repetition		25	50	
emittance	(e^-)	4×10^{-8}	6.4×10^{-8}	m
	(e^+)	8×10^{-7}	8.8×10^{-7}	m
energy width	(e^-)	0.2	0.125	%
	(e^+)	0.22	0.25	%
[MAIN ACCELERATOR]				
Accelerator section				
type of structure		T.W., $\frac{2}{3}\pi$-mode, semi-C.G.		
frequency		2856		MHz
disk aperture diameter		24.85∼ (75 μm step)		mm
length (with vacuum flanges)		2040		mm
filling time		0.5		μs
energy gain (no-load)		7.4		$MeV/MW^{1/2}$
total number		162	230	
Accelerator unit[*2]				
length (regular unit)		9.6		m
number (total)		46	57	
(before e^+ radiator)		3	26	
(stand-by and energy-tuning)		∼3+1	4+2	
energy gain (with RF compressor)			160	MV/unit
(without RF compressor)		62.5 (@20 MW)	90 (@40 MW)	MV/unit
energy multiplication			1.8	

Table 12.1(1): Changes in the major parameters of the linac from the present to KEKB.

	PRESENT	KEKB	
[PRE-INJECTOR]			
Gun			
type	triode		
cathode	BI-cathode (EIMACY796)		
high-voltage/width	200 kV/1μs		
grid-voltage/width	200 V/4 ns		
normalized emittance	$\sim 5 \times 10^{-6}$		m
1st-subharmonic buncher			
type of structure	re-entrant cavity		
frequency	119.000	114.2	MHz
field-strength	4	4	MV/m
2nd-subharmonic buncher			
type of structure	re-entrant cavity		
frequency		571.27	MHz
field-strength		4	MV/m
1st-prebuncher			
type of structure	T.W., $\frac{2}{3}\pi$, C.I.		
frequency	2856		MHz
cell number	7		
disk-aperture diameter	35.74		mm
phase velocity	0.7c		
shunt impedance	16.0		MΩ/m
2nd-prebuncher			
type of structure	T.W., $\frac{2}{3}\pi$, C.I.		
frequency	2856		MHz
cell number	5		
disk-aperture diameter	36.89		mm
phase velocity	0.7c		
shunt impedance	15.0		MΩ/m
Buncher			
type of structure	T.W., $\frac{2}{3}\pi$, C.G.		
frequency	2856		MHz
cell number	35		
disk-aperture diameter	35.0$\sim$19.3		mm
phase velocity	0.7c$\sim$1c		
shunt impedance	15.0		MΩ/m
Output beam			
energy	50	50	MeV
energy spread (σ_E/E)	0.6	0.6	%
normalized emittance	$\sim 6 \times 10^{-5}$		m

Table 12.1(2): Changes in the major parameters of the linac from the present to KEKB.

	PRESENT	KEKB	
[POSITRON PRODUCTION]			
Radiator			
material	Ta		
thickness (radiation length)	8 ($2X_0$)	16($4X_0$)	mm
diameter	8	8	mm
Primary electron			
energy	0.25	3.7	GeV
particle (charge)/pulse	1×10^{11}(16)	6×10^{10}(10)	(nC)
emittance (1σ)			m
energy with (σ_E/E)		0.45	%
Positron production rate			
after the solenoid (100 MeV)	6.5%		
at the 30° -transport (250 MeV)	4.2%		$\frac{e^+}{e^-GeV}$
final (2.5 GeV)	1.8%	>1.8%	
Focusing system			
type	QWT		
pulsed solenoid (strength×length)	2.3T×45 mm	2.3T×45 mm	
D.C. solenoid (strength×length)	0.4T×8 m		
normalized acceptance	6×10^{-3}		m

Table 12.1(3): Changes in the linac major parameters from the present to KEKB.

	PRESENT	KEKB	
[RF SOURCE]			
Modulator			
PFN charging voltage	45		kV
PFN total capacitance	0.3	0.6	μF
energy stored in PFN	300	600	J
pulse repetition rate	50		pps
PFN impedance	6.4	4.7	Ω
pulse width	3.5	5.6	μs
pulse output voltage	22.5		kV
pulse output power	80	107	MW
Pulse transformer			
step-up ratio	1:12	1:13.5	
2nd. voltage×width	0.95	1.7	Vs
core bias	none	necessary	
Klystron			
beam voltage	270	304	kV
beam current	295	352	A
rf power peak	33	46	MW
rf power average	3.3	9.3	kW
rf pulse width	2	4	μs
Pulse compression	none	SLED	
multiplication factor	1	$\sim$2	
Energy gain/unit	65	$\sim$160	MeV
[BEAM TRANSPORT]			
solenoids (injection)			
solenoids (e^+ generator)			
quadrupole triplets			
doublets			
singlets			
betatron wavelength			
[BEAM MONITORS]			
wall current monitor			
profile monitor (Ceramic)			
beam position monitor			
wire scanner			
core monitor			

Table 12.1(4): Changes in the major parameters of the linac from the present to KEKB.

12.1.2 RF Power Sources

The pulse modulators will be upgraded as indicated in Table 12.1(4). Ten new modulators will be added, while the existing units will be upgraded by replacing the IVRs, charging choke transformers, PFNs and thyratrons. To produce 4 μs pulses, two arrays of 20-section PFNs are used for each modulator. A schematic drawing of a modulator unit is shown in Fig. 12.2.

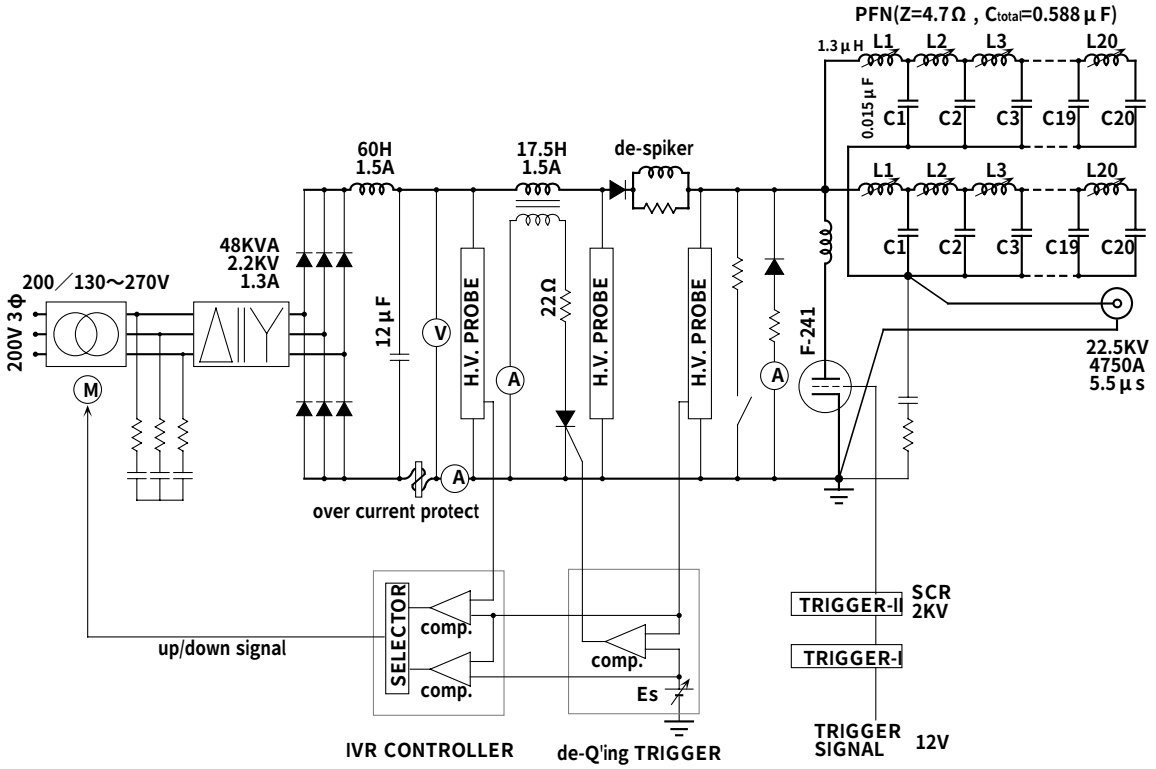

Figure 12.2: Modulator for the KEKB injector linac.

To produce the required 50 MW output power, an upgrade program of PV3030 klystron (30 MW type) is under way. The new klystron is called PV3030A3. Some of the specific features are:

1. The dimensions of the RF interaction region (cavity) are kept the same as those of PV3030, and hence, the same as SLAC XK-5 tubes.

2. The cathode diameter is increased from 80 mm to 85 mm, and the average pulse-current density from the cathode has been reduced.

3. A larger ceramic-seal is employed on the gun, in order to improve the high voltage capability.

4. The dimensions of the new klystron are similar to those of the original 30 MW type. This allows focusing magnets of previous types to be used with only minor modifications.

5. The distance between the anode and the 1st cavity was increased by 4 cm for stable microwave operations.

6. The space between the collector and its outer spool is increased, and a thicker X-ray shielding is inserted.

A test of PV3030A3 at a beam voltage of 310 kV has produced an output power of 51.5 MW with an efficiency of 44%.

In addition, a totally new 50 MW type klystron is under development. Figure 12.3 shows a comparison of cut-away views of the old and new tubes with an optimum magnetic field. Table 12.2 gives a comparison of the existing klystron and the new tubes.

	Unit	existing(PV3030)	PV3030A3	50MW
Beam voltage	kV	270	285(310)	315
Beam current	A	295	319(362)	370
Beam power	MW	80	91(112)	117
Beam pulse width	μs	3.5	5.5	5.5
Repetition rate	pps	50	50	50
RF output power peak	MW	33	40(50)	50
RF output power av.	kW	3.3	8.0	10
RF pulse width	μs	2	4	4
Efficiency	%	42	44	44
Perveance	$\mu A/V^{3/2}$	2.1	2.1	2.1
Overall length	mm	1317	1317	<1400
Number of cavity		5	5	5
RF window		single	single	single

Table 12.2: Parameters of the high power klystrons

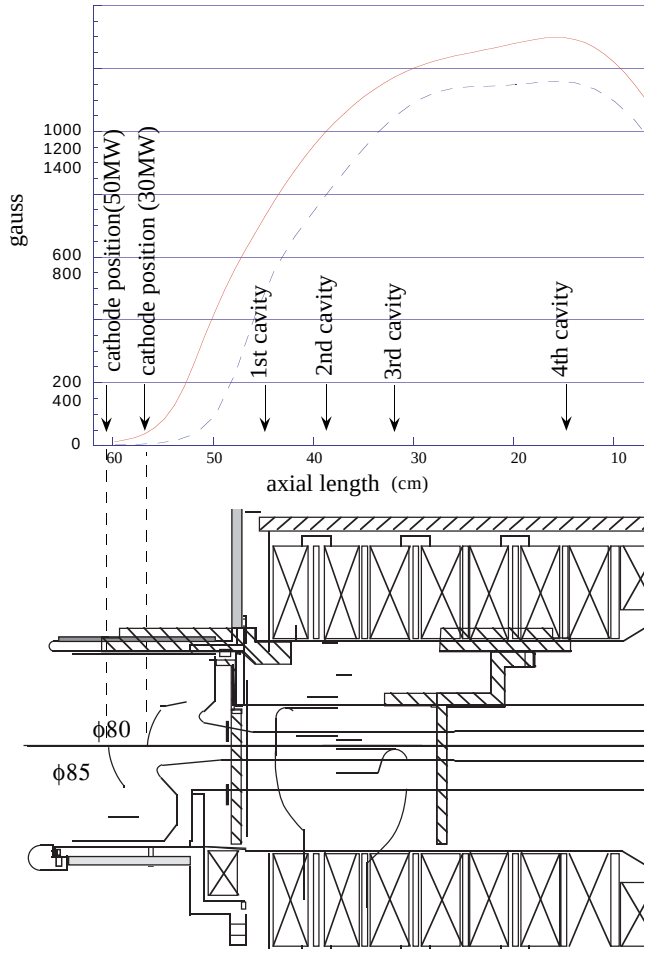

Figure 12.3: Comparison of a cut-away view of the old and new tubes with an optimum magnetic field.

The pulse transformers are being upgraded to provide a step-up ratio of 1 : 13.5 instead of the former 1 : 12. This is done by changing the winding ratio of the primary and secondary coils. To continue using the existing cores, which are rather large, a core-reset bias current to the primary windings will be applied. The insulation of the transformer will be improved to withstand a high voltage of over 310 kV during operation.

The existing pulse-transformer oil tanks will be reused. However, extension adapter tanks (10 cm high) will be added for mounting new klystrons with long gun insulators. All other parts, such as the feeder sockets, cooling pipes, klystron socket, heater transformer, and wave-form monitors, will be reused without modifications.

12.1.3 RF Pulse Compressor

The design of a SLED-type RF compressor has been developed to meet the specifications for KEKB. Table 12.3 summarizes its parameters. Five units have been fabricated so far. During an initial testing the RF power up to 48 MW was fed, and the energy gain was measured with and without the SLED to be 179 MeV and 97 MeV, respectively. The amplification of the accelerating energy was found to be > 1.85, as shown in Figure 12.4. The theoretically expected energy gain is 1.96 (see Figures 12.5(a)-(d)). A new RF-drive system is also being tested (Fig. 12.6).

Resonant mode	TE015
Q (theoretical)	105000
Q (measured)	100000
Coupling (type)	two-hole, side-wall
(β)	6.4
tuner	$<$ 2kHz/step (manual)
detuner (type)	solenoid-drive, needle (ϕ2mm, stroke 168mm)
(separation)	$>$20MHz
gain-shift	0.1%/5kHz(0.1°C)

Table 12.3: SLED specifications for the KEKB linac

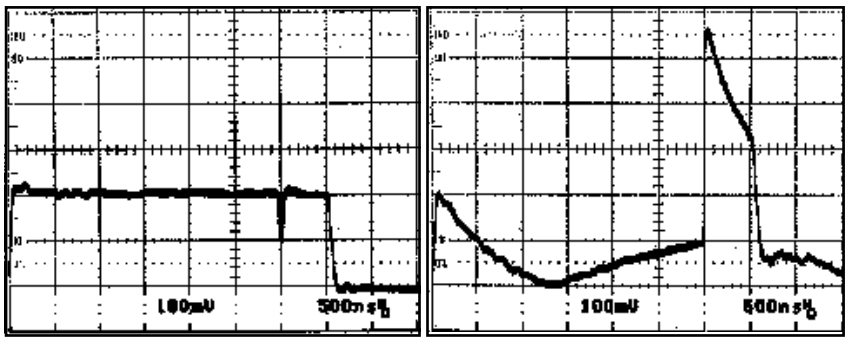

Figure 12.4: RF-pulse waveforms observed at an output port of the SLED.

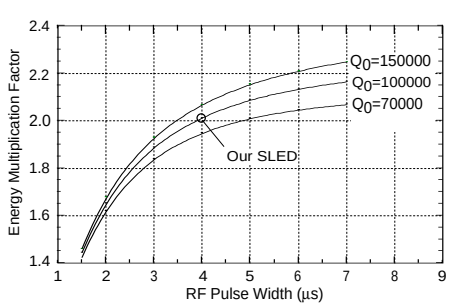

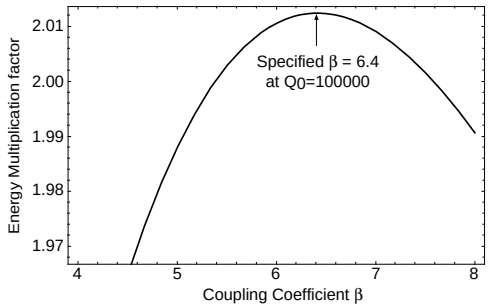

Figure 12.5(a): Energy multiplication factor as a function of the RF pulse width and the Q-value of the cavity.

Figure 12.5(b): Energy multiplication factor as a function of the coupling coefficient β.

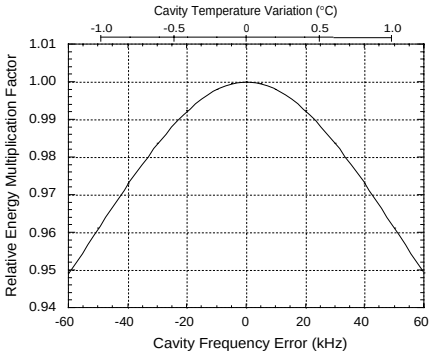

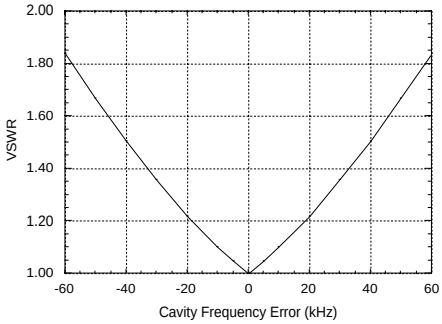

Figure 12.5(c): Relative energy multiplication factor as a function of the frequency error and temperature variation.

Figure 12.5(d): VSWR as a function of the frequency difference of the SLED cavities.

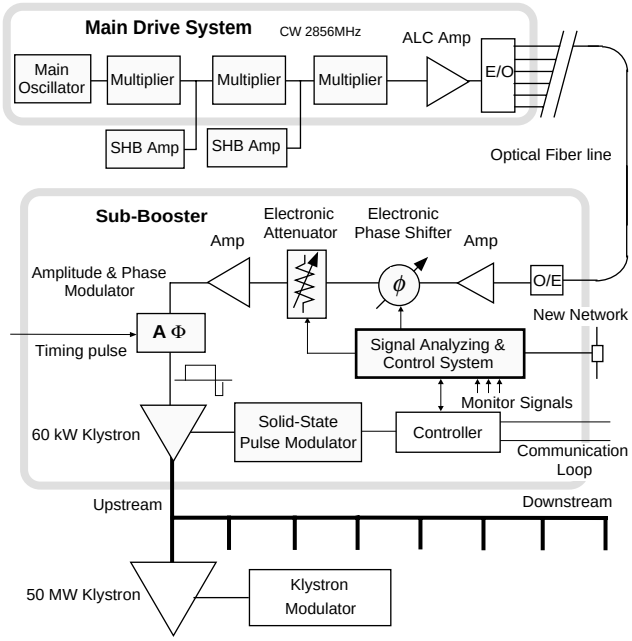

Figure 12.6: New rf drive system for the KEKB injector linac.

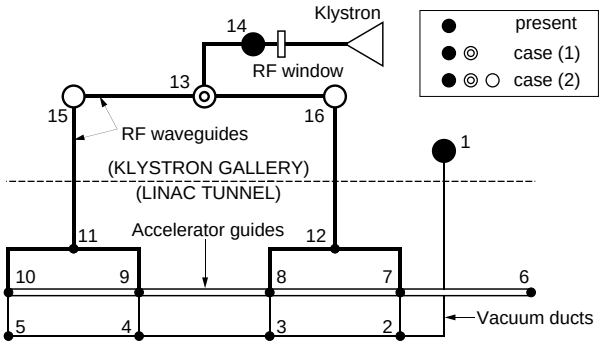

Figure 12.7: Schematic diagram of the vacuum network in an accelerator unit.

12.1.4 Vacuum Improvement for High-power Operation

To stably operate the linac under a very high-field strength (20 MeV/m) condition in the linac, the rf-conditioning may take a long time period. Also, electrical breakdown phenomena at the accelerator guides and the rf window are a concern.

The breakdown phenomena depend not only on the strength of the electric (accelerating) and magnetic (focusing) fields, but also on the surface and bulk conditions of the materials. Such surface conditions as contamination and adsorbed water molecules are generally correlated to the vacuum pressure. Therefore, the breakdown phenomena are often related to the vacuum quality in the system. For instance, klystron window breakdown is scarcely initiated from the inside of a klystron, where the pressure is lower than 1×10^{-6} Pa; window breakdown usually occurs on the waveguide side, where the pressure is typically $\sim 10^{-5}$ Pa. It is thus expected that a pressure reduction is one of the possible measures for suppressing various breakdown problems. A new method, which uses characteristic matrices of the vacuum network geometry, has been developed, and is used to analyze the pressure profile of the system.

We have investigated the changes of the pressure profile when some new pumps are added to the present system. Figures 12.7 shows the layout of the vacuum system. Two configurations have been tested initially: (1) A pump is added at node 13, and (2) three pumps are added at nodes 13, 15 and 16. Figure 12.8 shows the resultant pressure distribution.

Other configurations were then examined for a further reduction of the pressure (Figure 12.9). The configuration for case (3) is slightly different from that of case (2). A 500 ℓ/s pump is moved from the klystron gallery to the neighborhood of the accelerator guides in the tunnel; the length of the penetrating vacuum duct is shortened from 6 m to 1 m. In case (4), eleven pumps having an effective pumping speed of 10 ℓ/s are mounted at every node. The pressures at both ends of the accelerator guide are noticeably reduced in these configurations, as shown in Figure 12.10. Among these

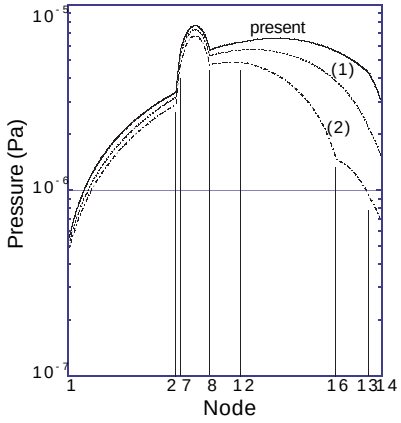

Figure 12.8: Pressure distributions calculated for the present configuration and for cases (1) and (2).

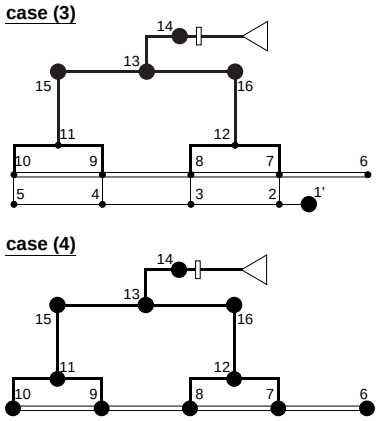

Figure 12.9: Configuration of the additionally installed pumps in the linac tunnel.

configurations, cases (2) and (3) are being tested in Sectors 4 and 2, respectively.

12.1.5 Beam Dynamics Issues

Longitudinal and Transverse Wakefields

To produce the required positron bunch population, intense electron bunches (10 nC with $\sigma_z = 1.5$ mm) need to be delivered on the positron production target at 3.7 GeV. With an accelerating gradient of 20 MV/m and a betatron wavelength of 40 m, the expected electron beam envelope in the upstream part of the injector is as shown in Figure 12.11(a),(b).

Due to the longitudinal wakefield, the energy broadening (σ_E/E) of the electron bunch for producing positrons is 1.2% when the bunch is on crest, and 0.45% when 7 degrees off crest (see Figure 12.12(a) and (b)). The average energy loss is 4 % as shown in Figure 12.13.

For stable operation of the system, the electron spot size on the positron production target needs to be less than 0.6 mm. Evaluations on the transverse wakefields indicate that to meet this requirement the beam displacement from the accelerator axis has

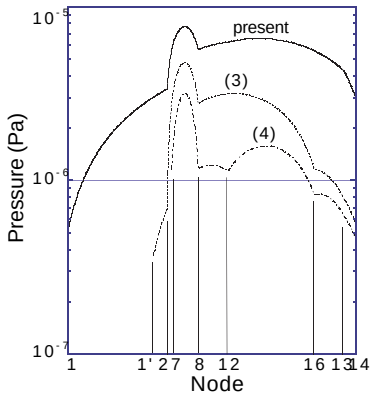

Figure 12.10: Pressure distributions calculated for cases (3) and (4).

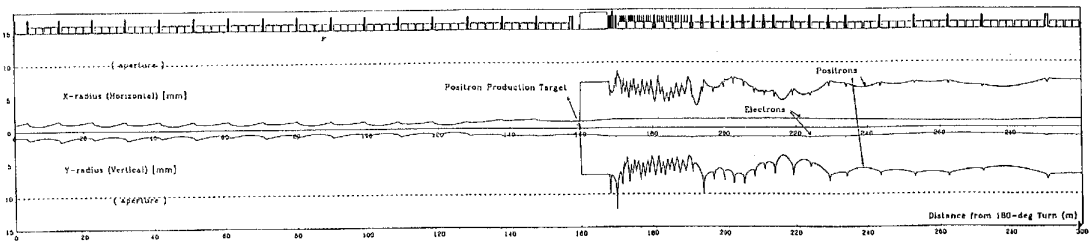

Figure 12.11(a): Calculated electron beam envelopes from the pre-injector (right side) to the 180° arc (left side).

Figure 12.11(b): Calculated electron beam envelopes after the 180° arc (left side) and positron beam envelopes after the positron production target (center).

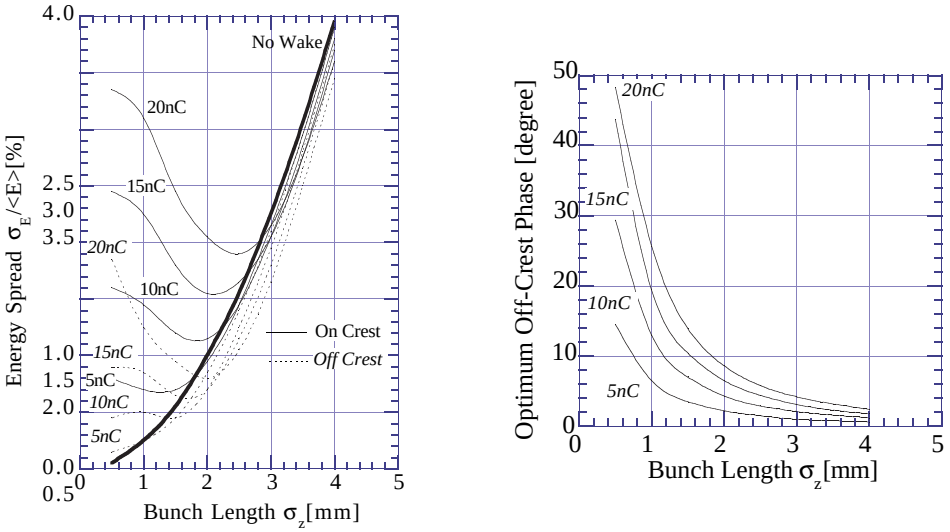

Figure 12.12(a): Bunch-length dependence of the energy spread.

Figure 12.12(b): Optimum off-crest phase as a function of the bunch length.

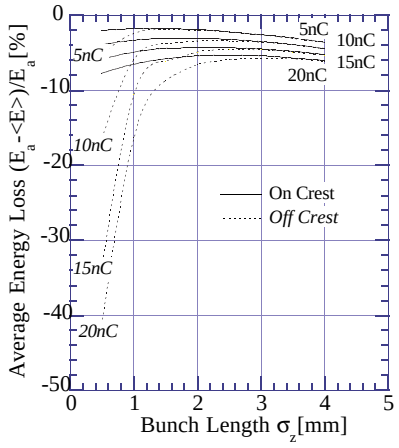

Figure 12.13: Average energy as a function of the bunch length.

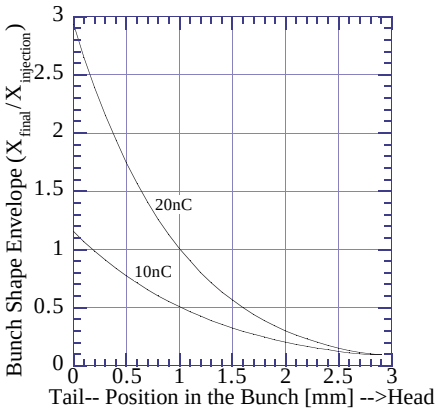

Figure 12.14: Bunch-shape deformation due to injection errors.

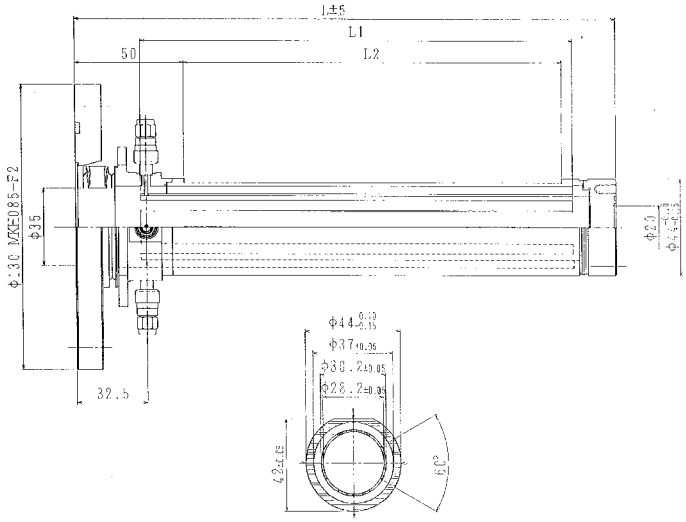

Figure 12.15: Beam position monitor (BPM) to be used in the KEKB injector linac.

to be kept below 0.5 mm. Good accelerator alignment and the beam position control must achieve and maintain this requirement.

Beam Position Measurement

From the discussion above, the accuracy of beam-position monitors (BPMs) is required to be ±0.1mm. Conventional strip-line monitors have been developed to be used at each quadrupole magnet. An electrode length of 130 mm has been tentatively chosen for testing, as shown in Figure 12.15.

The read-out electronics consists of the front-end, the detector and an external ADC, as shown in Figure 12.16. At the front-end the signal from an electrode is stretched in time by a band-pass filter (BPF), and is then amplified. At the detector the signal is split into the RF mixer port and the limiting amplifiers (L/A) to generate a local oscillator (LO). The peak value of the low-pass filtered intermediate-frequency (IF) signal is proportional to the beam-charge density and the beam position. The signal is captured by the sample-and-hold, and is digitized for computer processing where the horizontal and vertical displacements of the beam are calculated.

The required dynamic range of the signal processing circuit is 60 dB. Out of this, 35 dB is for the beam intensity measurement, and the remaining ±12 dB is for position measurements. This dynamic range covers the signal levels expected during regular operation, as well as during the commissioning period. A linearity better than 2% needs to be maintained. The measurements of test circuits indicate that those specifications can be met.

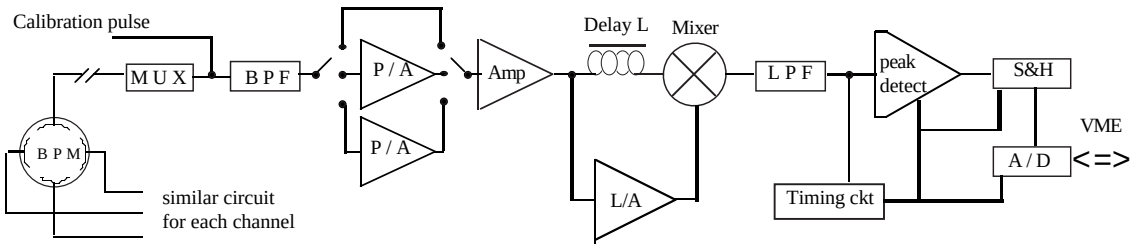

Figure 12.16: BPM circuit block diagram.

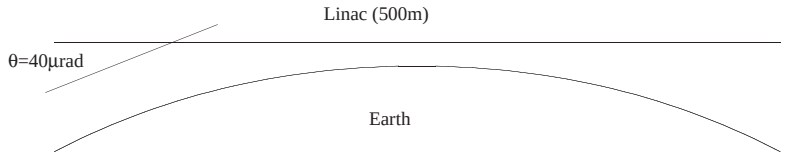

Figure 12.17: The linac is to be aligned tangential to the earth at its center.

Alignment of the J-shaped Linac Using a Laser System

The injector consists of two parallel linacs and a 180° bend arc section, as shown in Figure 12.1. A high-current beam from the upstream linac needs to be transported to the positron-production target without degradation of the beam quality. The alignment tolerance in the linac, according to beam dynamics calculations, is 0.1 mm. The downstream linac has a total length of 500 m, and the effect of the curvature of the earth is not negligible. The gravity observed at the center of the downstream linac defines its horizontal alignment, and, consequently, at its upstream end the linac has an angle of 40 μrad relative to the local horizontal plane defined by gravity. Figure 12.17 illustrates this fact.

Two methods for the injector alignment have been evaluated. The first method treats the three parts of the injector independently. In the second method a single common plane for the two linacs and the arc part is created as a reference. However, in this second method whenever the alignment of the downstream linac is changed, the rest of the system also must be changed. Therefore, the first method is favored and will be adopted. Although two vertical translation optics are required to join the entire injector, it is considered possible to achieve the required alignment accuracy.

The practical procedure for realizing this alignment is as follows. First, one must

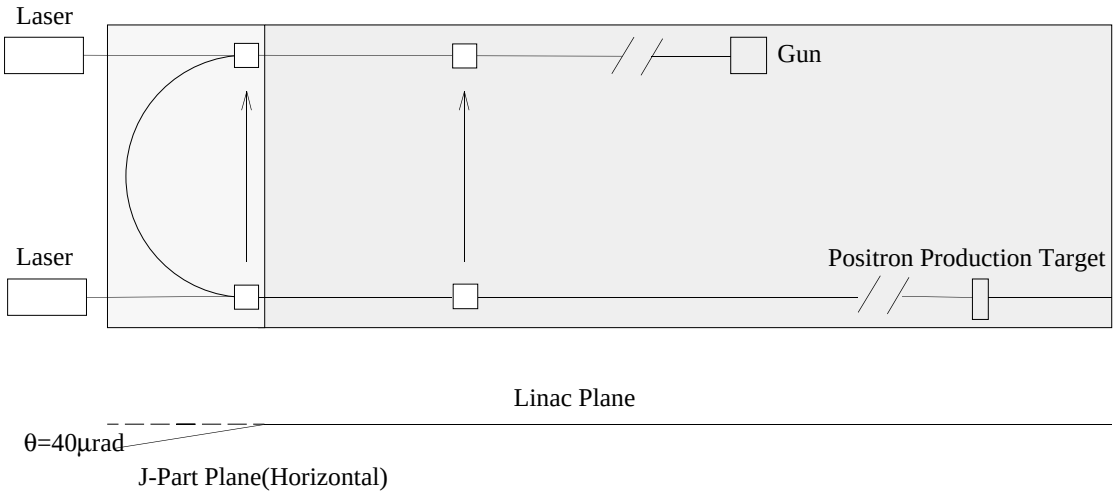

Figure 12.18: Alignment of two long linacs to be built parallel to each other.

establish a reference plane determined by the downstream linac by using the existing alignment system. A diffraction-limited laser beam defines the precise alignment axis along the entire downstream linac. Quadruple-type photo detectors placed on two ends of each support frame of the accelerator can detect vertical and horizontal position deviations with an accuracy better than 0.1 mm. All of the accelerator components are put on the support frames with a mechanical precision within 0.1 mm.

We then transfer two points of the downstream linac to the corresponding points of the upstream linac, as shown in Figure 12.18. This is done by using a laser beam, while using the usual levels for the direction perpendicular to the beam line. Based on these two points in the upstream linac as a reference, the laser alignment system is used in the same way as that of the downstream linac. Thus, one realizes the same plane for the two linacs with the same alignment precision.

Finally, the arc part is aligned in the horizontal plane by using levels. Because of the way that the "horizontal" alignment is defined for the upstream and downstream linacs, the plane of the arc part is inclined to that of the linac plane by 40 μrad.

After an initial alignment is carried out, continuous monitoring of the alignment status will be carried out by two sets of level-comparing systems for the upstream and downstream linacs. Clinometers will be installed at key locations, including the arc part.

12.1.6 Beam Control

Linac Operation Mode Regarding Electron and Positron Injection

Several schemes are being studied concerning the acceleration of electrons and positrons.

In the most straightforward scheme, the operating conditions for the electrons and

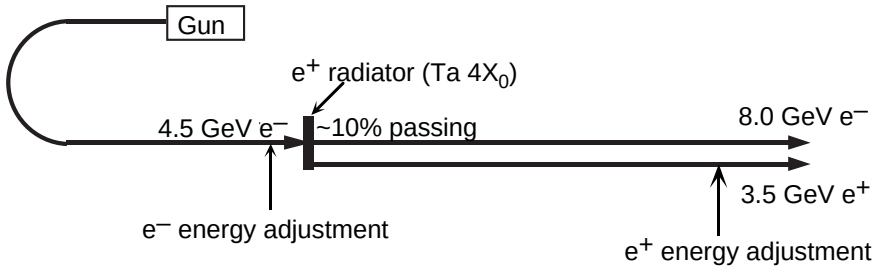

Figure 12.19: Simultaneous acceleration scheme of the electron and positron beams.

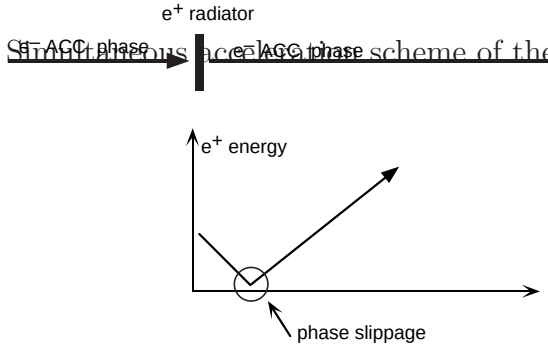

Figure 12.20: Acceleration phase adjustment of the electron/positron beams (Op.1), using phase slipping of the positrons in deceleration phase.

positrons are completely switched, and they are separately injected to HER and LER. This scheme provides optimized lattice focusing for the accelerated particles. However, many parameters, such as the RF timing and phases, need to be re-adjusted for both the upstream and downstream linacs.

In another scheme both the electron and positron beams are simultaneously accelerated and injected into the rings, as shown in Figure 12.19. The electrons are accelerated to 4.5 GeV by the first part of the injector. They then hit the positron production target. The emerging positrons are accelerated to 3.5 GeV. The target is built so as to have a small aperture which allows 10% of the electrons to pass through. Those electrons are accelerated in the downstream part up to 8 GeV. The electron and positron energies are adjusted at the end of the first and second parts, respectively.

In downstream part of the injector, the acceleration phases of the electrons and positrons should be 180° apart. This can be achieved by two methods. The first case is schematically shown in Figure 12.20: emerging positrons are first focused during their deceleration phase, but soon come to be accelerated because of phase-slippage. Figures 12.21(a) and 12.21(b) show a simulation of the capture rate and the longitudinal phase space of these positrons. Calculations indicate that 80% of the produced positrons can be accelerated; however, the energy spread will be larger than in the case with an optimum phase configuration.

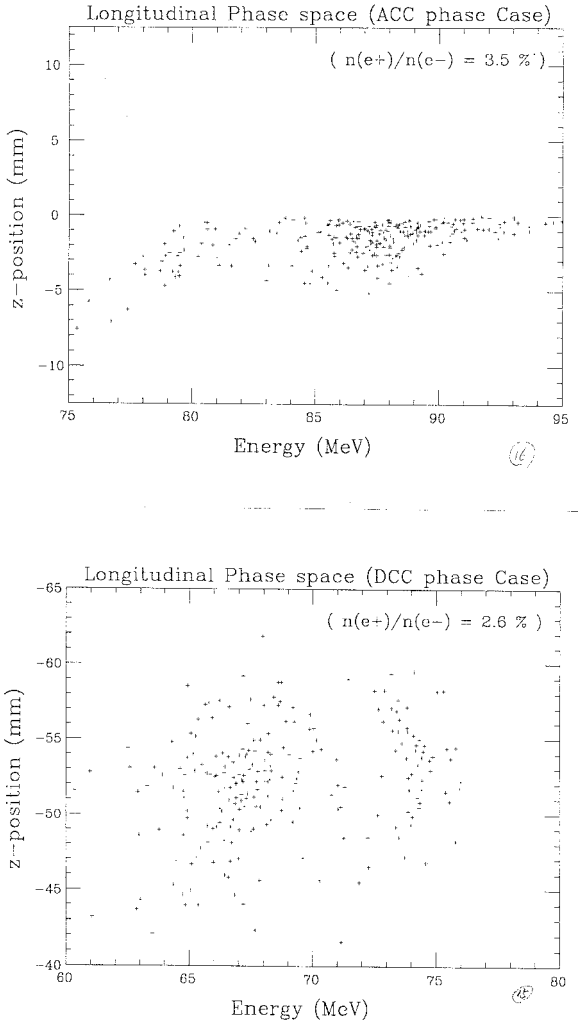

Figure 12.21(a): Longitudinal phase-space of the accepted positron beam (positron-acceleration phase).

Figure 12.21(b): Longitudinal phase-space of the accepted positron beam (positron-deceleration phase at first).

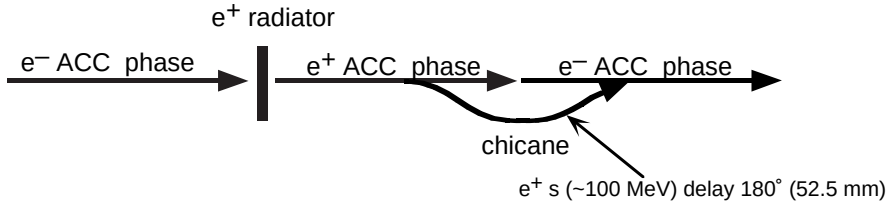

Figure 12.22: Acceleration phase adjustment of the electron/positron beams (Op.2), using a chicane to make phase-delay of positrons.

In the second case (shown in Figure 12.22) positrons are first focused in their acceleration phase, then their phase is shifted by 180° by separating them with a chicane. In the interval between the positron production target and the chicane, the electrons are slightly decelerated. However, its effect is negligible since the electron energy is larger than the positron energy there by a factor > 50.

If the two beam are co-accelerated, naturally the early part of the beam transport beam line needs to simultaneously deliver two beams of different energies. Studies are being prepared, regarding these issues as well as the bunching process during the phase-slippage.

Feedback to the Linac Beam Parameter

The beam energy in the injector is monitored at two locations: one in the arc section and the other after the linac.

In the arc section the nominal beam energy is 1.6 GeV. The energy fluctuation is detected with BPMs having a resolution of 0.03%. The beam energy there will be controlled by adjusting the phase of the last two klystrons of the upstream linac. Details of the correction algorithm are being considered.

At the end of the linac, electron and positron beams will be separated and transported independently. At the beam switch yard, the energies of both the electron and positron beams will be controlled in the same manner as in the arc section.

12.1.7 Schedule

The schedule for the upgrade is shown in Table 12.4. An important constraint is that injection to the PF ring has to be maintained during the upgrade project. Invasive work has to be done during the annual shutdown period each year. The upgrade of the present linac (from sector 1 to 5) and the construction of new sections (A, B, C and the arc section) will be conducted independently before June, 1998. After each portion is sufficiently tested, it will be connected during the summer shutdown of 1998. Commissioning of the 8 GeV linac will start in November, 1998.

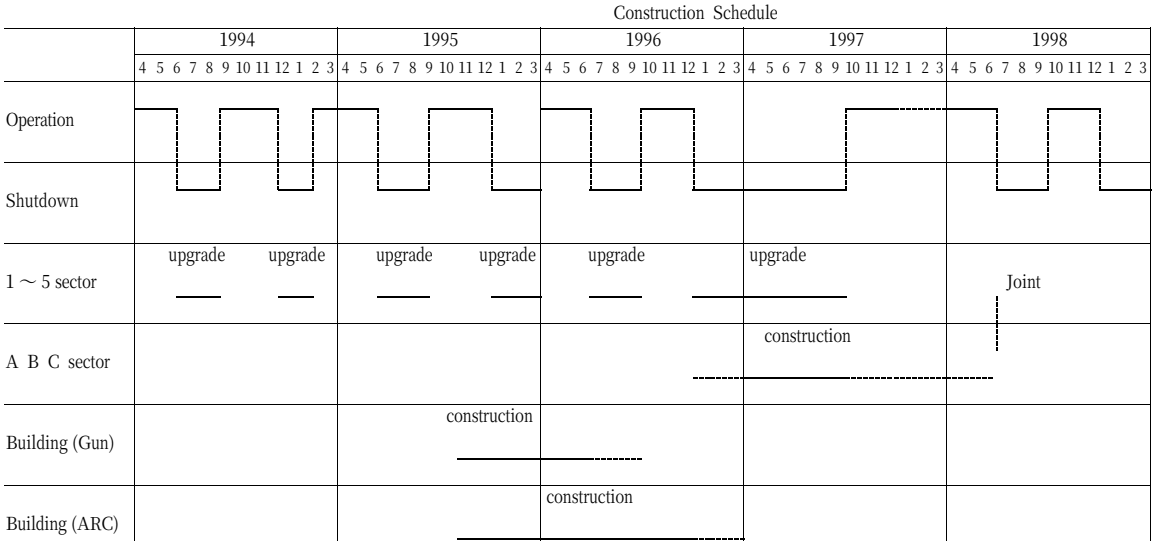

Table 12.4: The schedule of the injector upgrade program.

12.2 Average Luminosity

12.2.1 Beam Lifetime

In this section we evaluate the beam lifetime, which will be useful for simulating the optimum operation and the beam fill patterns of KEKB. The dominant sources of particle loss, which is responsible for the finite beam lifetime at KEKB, are the following three: the beam-beam bremsstrahlung in the beam collision, the beam-gas scattering and the Touschek effect.

The beam lifetime due to beam collisions depends on the energy acceptance $\Delta E/E$ of the ring. However, the dependence on $\Delta E/E$ is relatively small for $\Delta E/E$ >0.5%. For example, if the energy acceptance is increased from 1% to 2%, the lifetime varies from 8.8 hours to 10.7 in the LER, and from 20.9 hours to 25.3 in the HER. Since an optics study has shown the feasibility of an energy acceptance which exceeds 1% in both rings, it is reasonable to take the lifetime at the 1% acceptance.

The lifetime due to beam-gas scattering depends on the vacuum pressure, and again weakly on the energy acceptance. Assuming a design value pressure of 1×10^{-9} Torr and a 1% energy acceptance, the lifetime would be 45 hours in both rings.

The Touschek effect plays an important role in causing a beam loss in the LER. In this case, the lifetime depends strongly on the energy acceptance, as well as on the transverse acceptance. The expected acceptance of LER leads a Touschek lifetime of more than 15 hours. At this moment the LER lattice has not been completely finalized, and complete calculations of the expected acceptance, which include effects of machine errors, are not yet available. Consequently, the estimated Touschek lifetime should be considered to be a variable parameter for simulating the operation. It is noted that this effect does not contribute to the lifetime of the HER. Table 12.5 summarizes the beam lifetime estimation.

Table 12.5: Beam lifetime estimation for KEKB

	Beam-Beam	Beam-Gas	Touschek	Total
LER	20.9	45	5	3.7 h
			10	5.9 h
			15	7.3 h
HER	8.8	45	–	7.4 h

12.2.2 Operation Pattern

First, we estimate the initial fill time for KEKB. In what follows, the calculations are made based on the assumption that the positron and electron charges from the linac are 0.64 nC/pulse and 1.28 nC/pulse at 50 Hz, and that the injection efficiency to the KEKB rings is 50%. Then, for full-bunch operation the required injection time for the LER and HER will be 0.5 hours and 0.1 hours, respectively.

It should be noted that the beam intensity in the rings does not necessarily decay as an exponential function of time. Under stationary operation, the stored current will not decay very much before the next topping. Therefore, we use a simple model where the intensity decays exponentially with the estimated lifetime. Then the luminosity itself decays exponentially with a lifetime, τ_L, given by

$$\frac{1}{\tau_L} = \frac{1}{\tau_1} + \frac{1}{\tau_2},$$

where τ_1 and τ_2 are the lifetime for the LER and HER. With the refilling time T_F, and the experiment time T_E, the average luminosity would be

$$\overline{\mathcal{L}} = \frac{1}{T_F + T_E} \int_0^{T_E} \mathcal{L}_0 e^{-\frac{t}{\tau_L}} dt = \frac{\tau_L \mathcal{L}_0}{T_F + T_E} [1 - e^{-\frac{T_E}{\tau_L}}],$$

where $\mathcal{L}_0$ is the peak luminosity. The beam loss during the refill time has been neglected. The refill time is a sum of the injection time for the positrons and electrons, and the time that is needed for switching the operation mode between the injection and the physics run.

Figure 12.23 shows the average luminosity for three cases with the varying Touschek lifetime in LER. A mode switch time of 2 minutes is assumed. With a 10-hour Touschek lifetime, the average luminosity and the injection time would be as shown in Figure 12.24. Taking account of the number of bunches (5120) and the repetition rate of 50 Hz of the linac, we can see that at least 1.7 minutes are required to refill each bunch. The injection time will be a multiple of the minimum refilling time. We define the optimum operation pattern to be what gives an average luminosity to be $> 75\%$ of the peak luminosity. In Figure 12.24, such an optimum operation pattern would consist of a 40-minute physics data acquisition time and a 7-minute refill time, including both electrons and positrons. Each positron bunch would be recharged with two shots from the linac. Under this condition the operation pattern would look like the time chart in Figure 12.25.

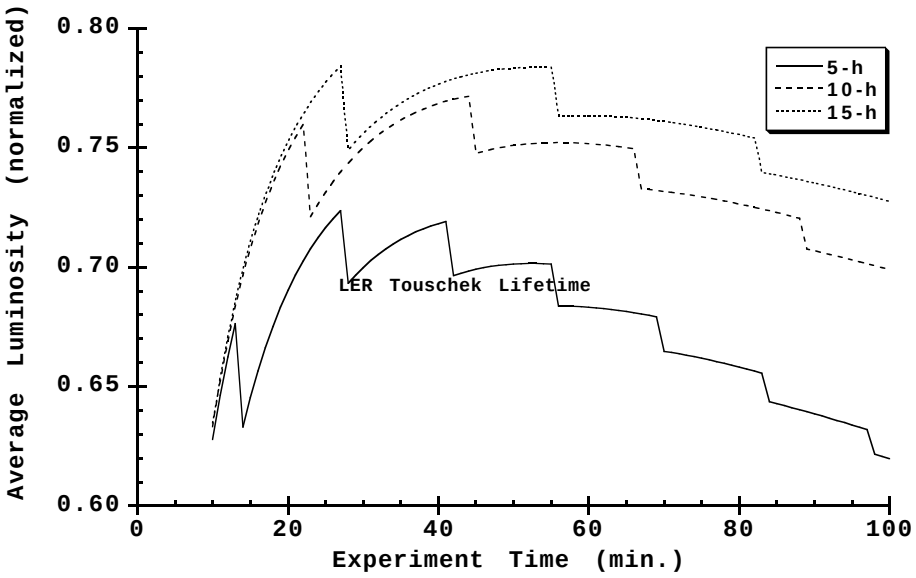

Figure 12.23: Average luminosity for different LER Touschek lifetimes.

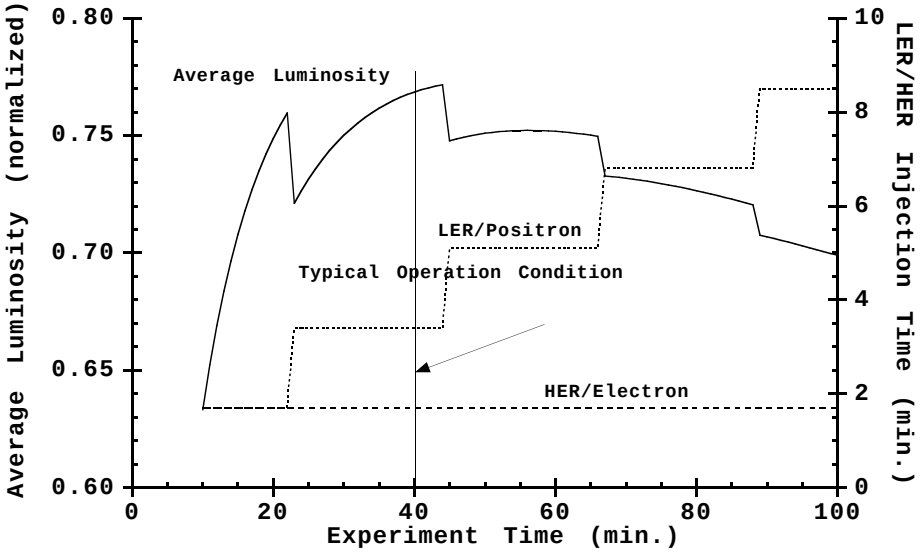

Figure 12.24: Average luminosity and injection times for the case of a 10-hour LER Touschek lifetime. The vertical line indicates a typical operation condition.

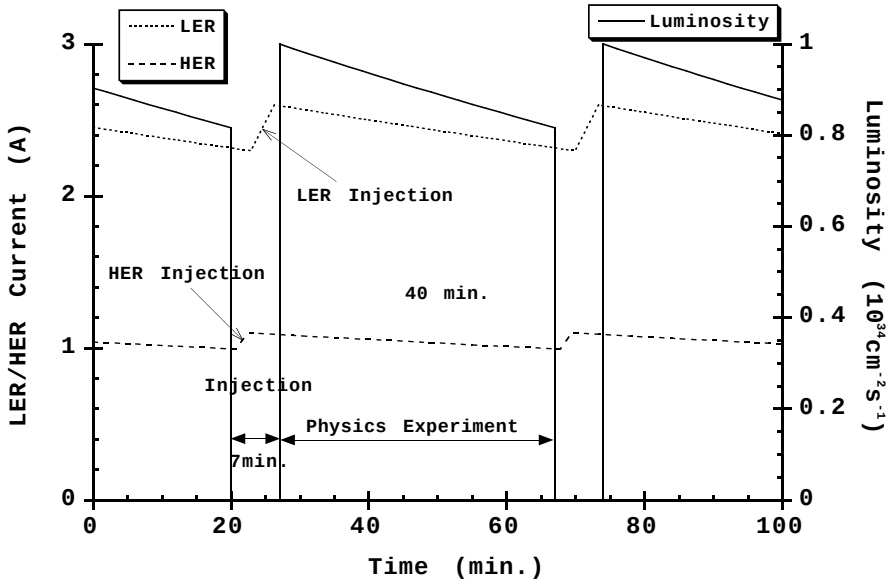

Figure 12.25: Luminosity and the LER/HER currents on the typical operation condition. The injection time includes the LER/HER topping times and the time period for changing the operation mode.

12.3 Beam Transport

12.3.1 Design Considerations

The parameters related to the beam transport (BT) between the linac and the KEKB rings are summarized in Table 12.6.

To minimize the construction cost, maximum use will be made of the existing tunnels for TRISTAN injection; the tunnels for both the TRISTAN accumulation ring (AR) injection and the TRISTAN main ring (MR) injection will be used. For injecting beams to the KEKB rings, the route as shown in Figure 12.26 has been chosen. This route is designed to avoid interference with the existing buildings for the AR.

Another important design consideration is operational simplicity. If a single beam line is used for both electrons and positrons having different energies, the need to re-adjust the magnet excitations or to switch their polarities tends to create various operational complications. Thus, in the BT design for KEKB, two beam lines will be implemented separately for the electrons and positrons. The beam lines have no common magnets nor common magnet power supplies, except for the first magnet that separates the two beams from the linac.

	e^-	e^+
Maximum energy [GeV]	8.4	3.7
Emittance(2σ) [m]	6.4×10^{-8}	8.8×10^{-7}
Energy Spread(2σ) [%]	±0.3	±0.5
with ECS		±0.25
Bunch length (σ_z) [mm]	1.5	1.5
with ECS		3.0
Time jitter $\Delta z_{max}/c$ (ps)	±30	±30
Momentum acceptance of Rings [%]	0.5†	0.5†

† 30 to 50 % degradation are assumed compared to the ideal case.

Table 12.6: Parameters relevant to the beam transport system. In the table, "ECS" means the energy compressor system for the positrons in the early part of the beam transport. See the text for details.

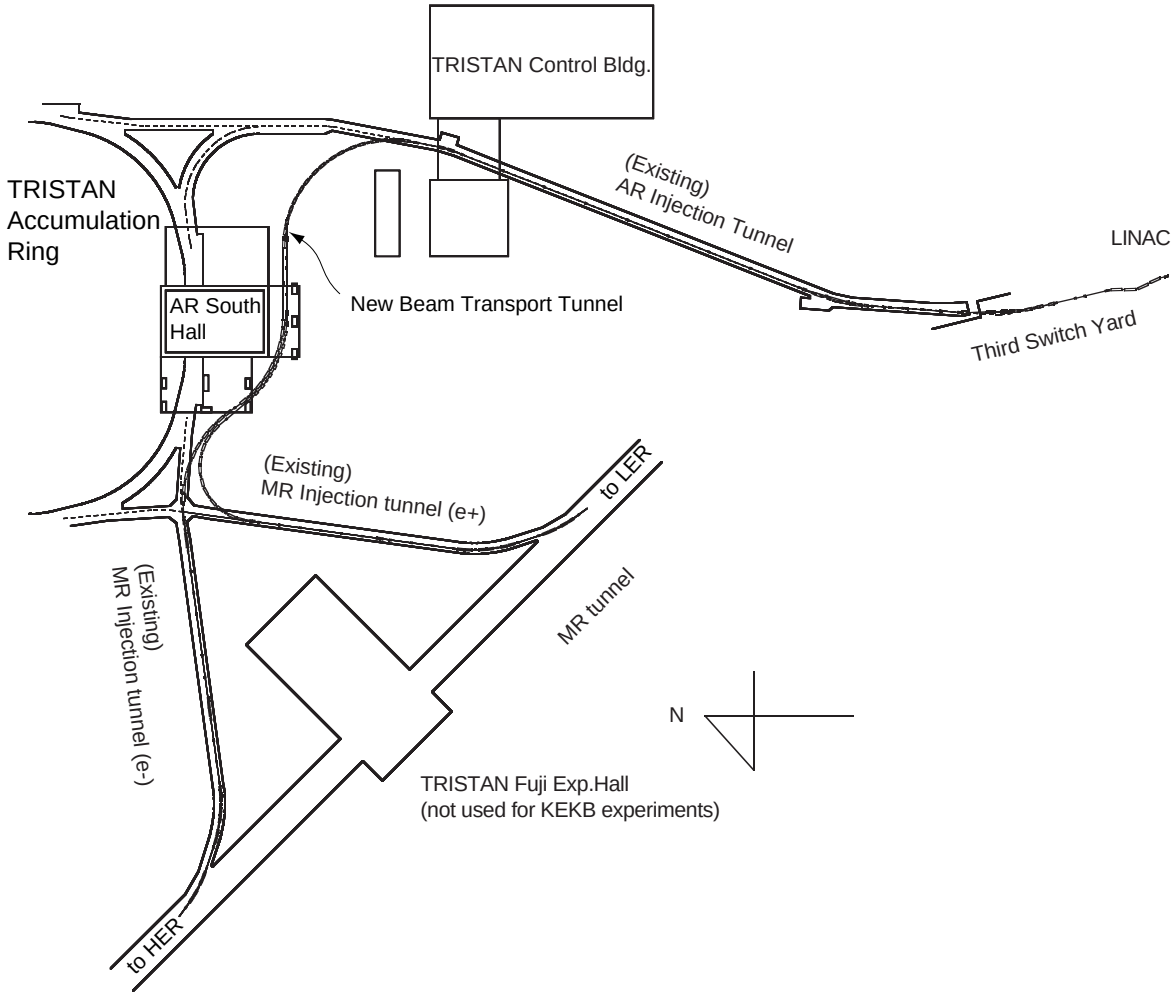

Figure 12.26: Layout of the beam transport lines.

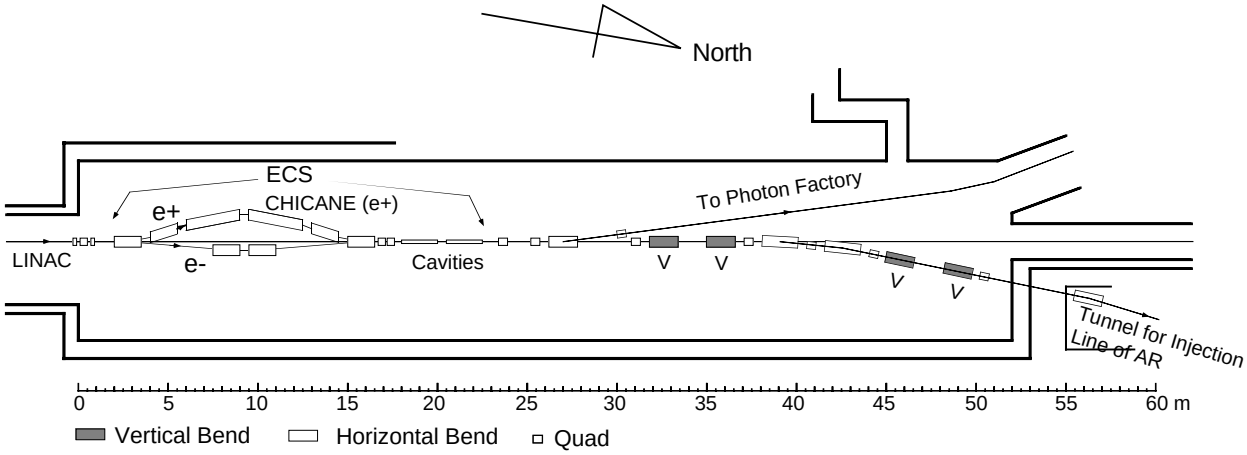

Figure 12.27: Layout of the Third Switch Yard.

12.3.2 Routing of the electron and positron beams

Figure 12.27 shows a part of the beam line which is immediately downstream of the linac exit before reaching the AR injection tunnel. This area is called the 3rd switch yard

In the upstream end of the 3rd switch yard, an energy compression system (ECS) will be implemented. Its purpose is to reduce the energy spread of the positrons from the linac by a factor of 1/2, and to relax the energy acceptance requirement for the LER. The ECS consists of a series of chicane dipole bends and two 2 m-long S-band accelerating structures. There will be no ECS specifically for electrons. The electrons are simply separated from the positrons, bypassing the positron ECS, and are brought back to the original line by two dipole magnets.

The AR injection tunnel does not have sufficient width to accommodate the two beam lines horizontally. The lines will be stacked vertically, with the positron line on top of the electron line in the AR injection tunnel. For this purpose, the two beams are separated by vertical dipole magnets in the downstream part of the 3rd switch yard. As shown in Figure 12.27, four dipole magnets will be used to make the vertical dispersion closed. With this manipulation, the vertical separation of two beams will be 0.6 m. The horizontal dipole magnets between the vertical ones will guide the beams to the new transport lines through the AR injection tunnel.

As shown in Figure 12.26, immediately after the first arc in the middle of the new tunnel the two lines are separated horizontally. The elevation of the positron line is reduced in the subsequent straight section to meet the MR injection tunnel at an appropriate point in the middle of the downward slope. The electron line maintains its level up to the entrance of the MR injection line. After passing the downward slopes, only minor modifications to the injection lines are required, since the injection points to the KEKB rings are at nearly the same position as those of the TRISTAN MR.

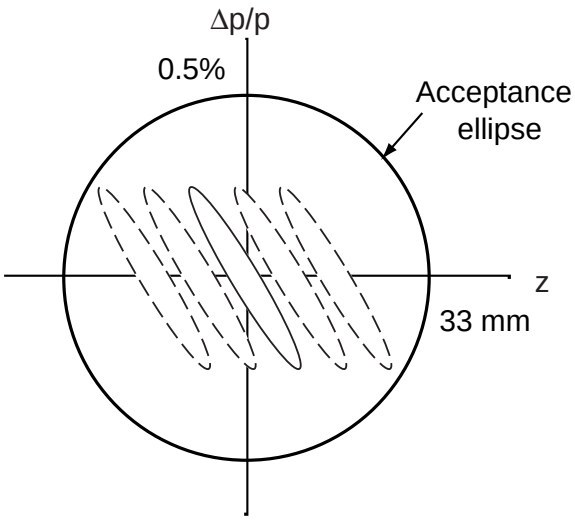

Figure 12.28: Acceptance of the LER and incoming beam. The large circle indicates the acceptance ellipse in the longitudinal plane of the LER. The rotated ellipse with a solid line represents the incoming positron beam with ECS, while the ellipses with broken lines indicate incoming beams with a timing jitter. The outermost ellipse corresponds to the maximum allowable jitter. R_{56} is assumed to be 4 m.

12.3.3 Constraints to R_{56} and the tolerance of timing jitter

The ECS may not be operational in the initial KEKB operation. In that case, the positron beam will have a large energy spread ($\sigma_\epsilon = 0.25\%$ without ECS). While the original bunch length expected from the linac is 1.5 mm, a bunch lengthening effect through the $\sigma_\epsilon R_{56}$ term needs to be considered. Here, the R_{56} refers to the (5, 6) component of the transfer matrix, i.e. the path length dependence on the momentum. For example, if the R_{56} term of the BT exceeds 5 m, the bunch length will be larger than 12.5 mm. The beam with a large bunch length induces a large quadrupole synchrotron oscillation after injection. Similarly, any timing jitter of the injected beam also induces (dipole) synchrotron oscillations. Figure 12.28 illustrates the acceptance ellipse for injection and possible patterns of a mismatch.

The largest amplitude of the induced bunch oscillation immediately after injection thus depends on R_{56}. Figure 12.29(a) shows the largest amplitude of energy oscillation as a function of R_{56}. Figure 12.29(b) shows the timing jitter tolerances as a function of R_{56}, which was defined as the largest longitudinal position shift that makes the beam ellipse cross with the acceptance boundary.

It is seen that the timing jitter tolerance is zero for the case of positrons without ECS. For positrons with ECS, a jitter tolerance of 30 ps (9 mm) demands that R_{56} be less than 7.5 m. For electrons, R_{56} should be less than 6 m. The optics design of BT

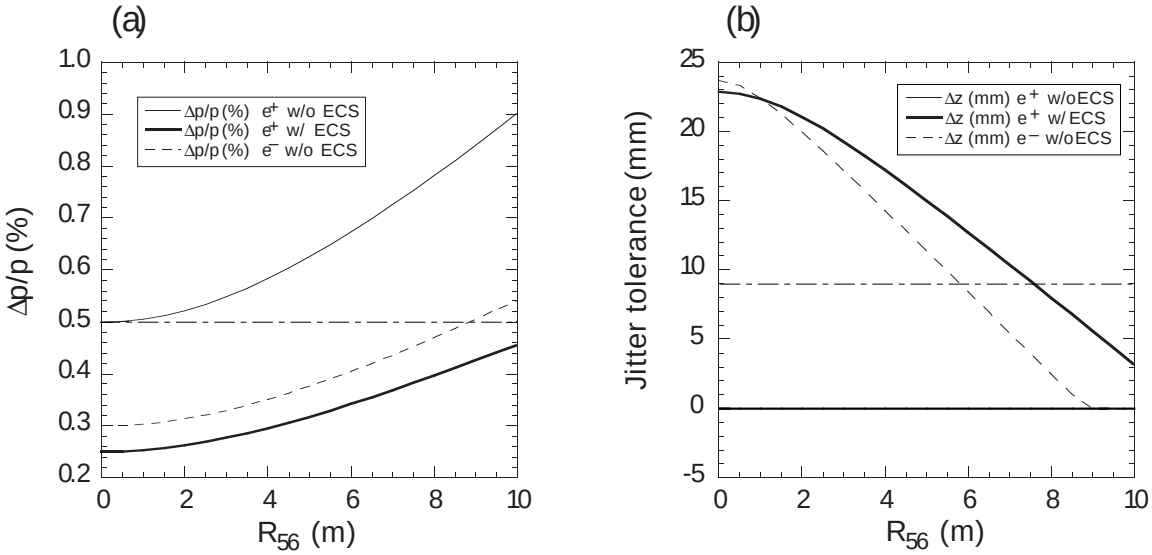

Figure 12.29: (a) Largest amplitude of energy oscillation as a function of R_{56}. The dash-dot line shows a momentum acceptance of 0.5%. (b) the timing jitter tolerances as a function of R_{56}. The broken line shows a tolerance of 9 mm (30 ps).

has been made such that the value of R_{56} will be 4 m.

It should be noted that R_{56} can be written as

$$R_{56} = \Theta\bar{\eta}, \tag{12.1}$$

where Θ is the total bending angle and $\bar{\eta}$ is the average dispersion in the dipole magnets. From this it is found that $\bar{\eta}$ needs to be smaller than 1.2 m for the positron line to satisfy $R_{56} = 4$ m.

Since the BT arc is occupied by strong dipole magnets of 1.5 T, there is no room to make the dispersion below 1.2 m for each arc. Consequently, another approach to suppress the R_{56} has been taken for this BT design: the optics around the three arcs in the new BT tunnel are arranged such that the arcs in the upstream generate negative dispersion at the downstream arcs so that R_{56} of the downstream arcs is decreased.

In the current design the electron line will require 54 dipole and 62 quadrupole magnets; the positron line will require 57 dipole and 64 quadrupole magnets. Some of the magnets, particularly the magnets in the downward slopes, may be recycled from the TRISTAN injection beam line.